HHS Public Access

Author manuscript

Adv Mater. Author manuscript; available in PMC 2019 May 01.

Published in final edited form as:

Adv Mater. 2018 May ; 30(22): e1800001. doi:10.1002/adma.201800001.

Desktop-Stereolithography 3D-Printing of a Poly(dimethylsiloxane)-based Material with Sylgard-184 Properties

Dr. Nirveek Bhattacharjee, **Dr. Cesar Parra-Cabrera**, **Dr. Yong Tae Kim**, **Alexandra Kuo**, and **Prof. Albert Folch**

Department of Bioengineering, University of Washington, 3720 15th Ave NE, Foege, Building N423A, Seattle, WA 98195, United States of America

Abstract

The advantageous physiochemical properties of poly(dimethylsiloxane) (PDMS) have made it an extremely useful material for prototyping in various technological, scientific, and clinical areas. However, PDMS molding is a manual procedure and requires tedious assembly steps, especially for three-dimensional (3D) designs, thereby limiting its access and usability. On the other hand, automated digital manufacturing processes such as stereolithography (SL) enable true 3D design and fabrication. Here we report the formulation, characterization and SL application of a 3D-printable PDMS resin (3DP-PDMS) based on commercially available PDMS-methacrylate macromers, a high-efficiency photoinitiator and a high-absorbance photosensitizer. Using a desktop SL-printer, we demonstrate optically transparent sub-millimeter structures and microfluidic channels. We also used an optimized blend of PDMS-methacrylate macromers to SL-print structures with mechanical properties similar to conventional thermally cured PDMS (Sylgard-184). Furthermore, we show that SL-printed 3DP-PDMS substrates can be rendered suitable for mammalian cell culture. The 3DP-PDMS resin enables assembly-free, automated, digital manufacturing of PDMS, which should facilitate the prototyping of devices for microfluidics, organ-on-chip platforms, soft robotics, flexible electronics and sensors, among others.

Summary

A PDMS-based stereolithography resin for 3D-printing transparent, flexible, biocompatible, high resolution elastomeric structures with mechanical properties similar to Sylgard-184 PDMS is reported. A 3D-printed microfluidic device showing a heterogeneous laminar flow is demonstrated. The resin is formulated for use with affordable desktop stereolithography printers so that rapid prototyping and digital manufacturing of microdevices can become more accessible.

Graphical Abstract

Supporting Information

Supporting Information is available from the Wiley Online Library or from the author.

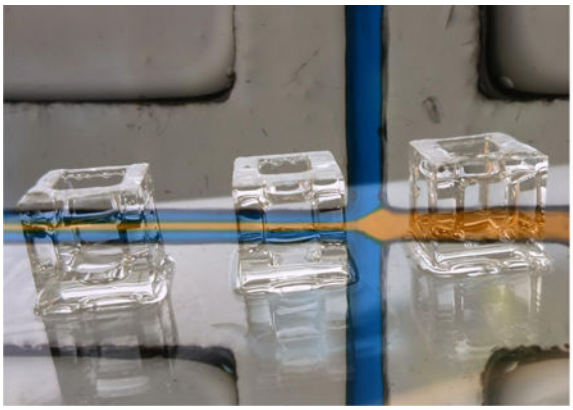

Keywords

pdms; poly(dimethylsiloxane); 3d-printing; stereolithography; microfluidics

Poly(dimethyl-siloxane) (PDMS) has been widely used for prototyping devices for biomedicine, physics chemistry, and virtually every engineering discipline in the last two decades[1]. The popularity of PDMS can largely be attributed to its attractive material properties – it is transparent, elastomeric, biocompatible, gas-permeable, water-impermeable, and relatively inexpensive. PDMS (Sylgard-184) microdevices have traditionally been fabricated using soft lithography, a technique based on manual procedures consisting of micromolding, alignment and bonding of 2D layers, and inlet fabrication. Soft lithography's requirement for intensive manual labor results in expensive devices and hinders technology dissemination; its limitation to 2D layers restricts the 3D complexity of the structures that can be realized. 3D-printing, in contrast, is a family of automated, assembly-free manufacturing techniques for 3D digital designs that are now increasingly being used for fabricating devices because of their low cost and 3D design efficiency[2]. PDMS has been previously 3D-printed with extrusion-based printers at low resolution and diminished transparency[3–6]. Several desktop 3D-printers often use photopolymerization-based stereolithographic (SL) approaches in combination with photosensitive acrylate or epoxy resins[7]. Photocurable PDMS has been explored before in photolithography to make 2D structures[8–11]; however these resins often use photoinitiators that mostly absorb at shorter UV wavelengths (< 365 nm), which are currently unavailable in standard desktop SL-printers. Multi-photon micro-stereolithography and direct laser writing has been used to fabricate high-resolution (~1–5 μm) 3D structures made of PDMS doped with photoinitiators[12,13], but the fabrication rates are very slow and the two-photon laser setups are very expensive. A few commercial elastomeric SL-resins exist for desktop SL-printers (Formlabs Flexible, Stratasys TangoPlus, Spot-A-Elastic, Carbon EPU-40 and SIL), but their proprietary formulations preclude any customization of properties. Recently, some open-source siloxane-based SL-resins with improved elastomeric properties have been developed and used to print pneumatic actuators with digital light processing (DLP) SL[14,15]. However, none of these commercial or open-source resins have demonstrated the transparency, biocompatibility and elasticity of Sylgard-184 PDMS, all together. Here we report the stereolithographic 3D-printing of PDMS parts from a methacrylate-based resin

that can be photopolymerized with 385 nm UV light. This 3D-printable PDMS (3DP-PDMS) has all the advantageous properties of thermally-cured (Sylgard-184) PDMS.

In order to SL-print PDMS devices, we set out to formulate a 3DP-PDMS resin that would be: (a) photopolymerizable with high efficiency at longer UV wavelengths (385–405 nm) available in desktop SL-printers, (b) highly absorbent at the wavelength of the SL-printer, (c) with a viscosity low enough that uncured resin can be drained from at least millimeter-sized voids/channels, and (d) polymerizable into a material of similar properties as Sylgard-184 – i.e. optically transparent, gas-permeable, biocompatible, and highly elastic (can be stretched to more than 100% of its original length without breaking).

Acrylated and methacrylated macromers have been widely used to generate polymers with free radical photopolymerization[16,17]. We explored the use of two commercially-available silicone methacrylate macromers as the starting material for our resin: (1) a single PDMS polymer chain terminated on both ends with methacryloxypropyl groups (henceforth, referred to as 3DP-PDMS-E for end-terminal groups) (Figure S1a, Supporting Information), and (2) a co-polymer of 3-methacryloxypropyl-PDMS and PDMS, which leads to a few reactive methacryloxypropyl groups attached as side-chains along the PDMS-chain (henceforth, referred to as 3DP-PDMS-S, for side-chain groups) (Figure S1b, Supporting Information). Although macromers can be synthesized with different chain lengths as well as mixed at different percentages, for simplicity we restricted ourselves to commercially-available components (Table S1, Supporting Information).

The photoinitiator for the 3DP-PDMS resin had to satisfy the following criteria: (a) be readily soluble in silicone, (b) absorb strongly at 385 nm (the shortest wavelength UV-LED projector that can be fitted to commercial desktop SL-printers), and (c) be an efficient free radical generator. The requirement of a strong absorbance at 385 nm limited the number of photoinitiator options to several phosphine-oxide derivatives[18], of which ethyl (2,4,6-trimethylbenzoyl) phenyl phosphinate (TPO-L) (Figure S1c, Supporting Information), a Type I photoinitiator[18,19], is the only one that readily dissolves in PDMS. TPO-L is a yellow-colored viscous liquid, but at low concentrations (0.6%) it does not cause any appreciable deterioration to the optical transparency of the liquid PDMS-based resin. However, the transparency of a SL-printed structure also depends on the absence of surface roughness and bulk volume defects. To make transparent prints, we build the structures on a smooth glass slide derivatized with 3-(trimethoxysilyl)propyl methacrylate (TMSPMA), as described in our previous work[20]. Using a blend of 3DP-PDMS-S and 0.6% TPO-L, we were able to SL-print completely transparent elastomeric macro-structures (unlike previously-reported extrusion-printed translucent PDMS structures[3,5,6,21]), like cubes, hollow cubes and hollow tetrahedrons (Figure 1a and Movie S1, Supporting Information). Note that the hollow structures are not easily moldable. To quantitatively evaluate transparency, we used a spectrophotometer to compare the transmittance of rectangular pieces molded with Sylgard-184 and printed with 3DP-PDMS-S. While the freshly printed 3DP-PDMS-S pieces absorbed strongly at wavelengths less than 400 nm, their transmittance improved significantly when extracted with solvents (isopropyl alcohol (IPA) or Dynasolve M10 (M10)) overnight (Figure 1d). In the visible spectrum (400–700 nm), the solvent-extracted 3DP-PDMS-S parts matched the transmittance of molded Sylgard-184 pieces,

which is also evident when these pieces were placed over printed text and color images (Figure 1e).

Printing resolution is of critical importance for manufacturing microdevices. Our desktop SL-printer uses a DLP projector to print the features. Printing resolution in DLP-SL depends on the projected pixel width in XY (in our case, 52 μm), the minimum Z-layer thickness (as given by the Z-motor displacement resolution), the UV exposure conditions, and resin properties like monomer reactivity, optical absorbance, photochemical efficiency, and radical diffusivity[22]. We studied, characterized and optimized some of these different parameters in order to enhance the resolution of printing, without compromising on the optical clarity of the prints.

Since, irrespective of the macromer composition, the exposure time required for curing each layer (50 μm thick) of 3DP-PDMS is long (several seconds), reaction-diffusion kinetics play a role in the printable XY-resolution of straight lines and gaps[23]. In order to test the actual XY-resolution of printing, we printed 10 sets of 5 lines having the same width and separation distance (for example, 50 μm-wide lines separated by a 50 μm gap). The line and gap width of the sets were increased from 50 to 500 μm (1 to 10 pixels), in steps of 50 μm (1 pixel) (Figure S2a, Supporting Information). The printed 500 μm and 250 μm-wide lines were distinct and separate (representative magnified top and side-view micrographs are shown in Figure S2b-e, Supporting Information), but were ~15% and ~50% wider than designed for the 500 μm and 250 μm lines respectively. Gaps below 200 μm could not be resolved. However, the borders between individual pixels (inside the DLP, each pixel is represented by a micromirror) can be clearly distinguished at a higher magnification (Figure S2f, Supporting Information), suggesting that XY resolutions better than 50 μm are possible.

In SL, the effective Z-resolution of a print with overhanging structures is not only constrained by the Z-motor resolution, but also governed by the resin's optical absorbance and photopolymerization kinetics. For example, when the roof of a microfluidic channel is being printed, the light can penetrate into the underlying space, polymerize the resin and thereby result in an occluded microchannel. Hence the Z-resolution of a microchannel depends on the penetration depth of the specific wavelength of light into the resin[24]. Additives that absorb light without generating free radicals have been used before to increase the absorptivity of other SL resins[25,26]. However, many of the additives (e.g. Sudan I) absorb in the visible spectrum and make the prints colored[25]. We use isopropyl-thioxanthone (ITX) (Figure S1d, Supporting Information), which is a light yellow powder that dissolves in PDMS when solubilized first in tetrahydrofuran (THF). ITX has an absorption peak at 385 nm and a molar extinction coefficient of 5155 $M^{-1}cm^{-1}$ at 385 nm, which is ~15x that of TPO-L (343.74 $M^{-1}cm^{-1}$ at 385 nm) (Figure 2a). ITX is a photosensitizer and a Type II photoinitiator[19]. However the ketyl radical photo-product from ITX has poor reactivity towards acrylates[18]; therefore in our resin its main role is to limit the characteristic penetration depth at the wavelength where photopolymerization is triggered.

The characteristic penetration depth of the resin can be obtained from measurements of the cure-depth (thickness of polymerized resin) z_C, at different exposure times t_C, according to

the following equation that can be derived from the Beer-Lambert law (Supporting Information)

$$z_c = h_p \mathrm{In}\left(\frac{t_c}{T_o}\right) \quad (1)$$

where T_0 is the threshold time needed to cure the resin at maximum intensity and h_p is the characteristic penetration depth[24].

By measuring and plotting the cure-depths at different exposure times for a particular resin composition (Figure 2b&c), we analyzed the role played by the photosensitizer (ITX) in reducing the penetration depth. At constant photoinitiator (TPO-L) concentration (0.6% w/w), the penetration depth decreases by ~35% when ITX concentration is increased from 0 to 0.3%. A further increase of the photoinitiator and photosensitizer concentrations by 66% reduces the penetration depth by another ~16% (Table S2, Supporting Information). However, with an increase in the concentrations of the photosensitive components, the prints start getting more whitish and translucent. Therefore, for all subsequent prints using the 3DP-PDMS-S resin, we used 0.6% TPO-L and 0.3% ITX as the resin's components.

Our next goal was to SL-print microfluidic channels. We first studied the exposures needed to form roofs over channel voids by building test bridge structures (Figure 3a). We measured the thickness of the roofs from optical micrographs; for example, a 2.0 s exposure produced a ~330 μm roof (Figure 3a). To limit the resin in the channel voids from repeated exposure, we first built the walls of the device and then created the roof with a single exposure. To remove the uncured resin from the channels, we vacuum-aspirated the channels to remove excess resin followed by flushing of the channels with Dynasolve M10 and IPA while the entire device was submerged in IPA. This process was done in the dark and was repeated about 5–6 times until the channels were clear. Using these protocols, we were able to SL-print a simple 500 μm-wide microfluidic channel featuring three inputs and one output (Figure 3b). The device was completely transparent as seen from Figure 3b where the channels are filled with aqueous dyes. Figure 3c shows a heterogeneous laminar flow of yellow and blue dyes, both injected at 9 mL/hr into the device. With rapidly improving projector technology, the total pixel area is expected to decrease ~8.1-fold in the near future when the HD standard (1280 × 800 pixels, used in this study) is superseded by the 4K standard (3840 × 2160 pixels), which will result in a concomitant improvement in the channel resolution.

Low Young's modulus and high elongation-at-break are key properties of thermally cured PDMS that make it an ideal polymer for developing devices with elastomeric sensors such as microneedles for cell traction measurements[27] and actuators for microfluidic automation (valves and pumps)[28–30]. While the 3DP-PDMS-S macromer alone was sufficient for SL-printing macro-structures with low Young's modulus, we had to further optimize the resin formulation to make elastomers with elongation-at-break values similar to thermally cured Sylgard-184.

We were inspired by the crosslinking strategy in thermally cured PDMS (Sylgard-184), where vinyl groups at the terminal ends of a PDMS macromer reacts with the silicon hydride groups present along another PDMS macromer backbone to form a network structure. The stiffness of the final cross-linked polymer is determined by the ratio of the two PDMS macromers. Hence we explored different ratios of 3DP-PDMS-E and 3DP-PDMS-S (Figure S1a&b, Supporting Information), together with different photoinitiator concentrations, to optimize a formulation that can form polymers having Young's modulus (~1 MPa) and elongation-at-break (~140%) similar to structures molded with Sylgard-184. Optimal blends of the two macromers resulted in flexible structures that could be bent repeatedly over 180°, twisted and pulled without breaking (Figure 4a and Movie S2, Supporting Information). We performed classical tensile stress-strain measurements on materials made with different 3DP-PDMS-E:3DP-PDMS-S ratios by weight (henceforth termed E:S ratios) (Figure S3, Supporting Information). Representative stress-strain curves for different E:S ratio (4, 7, 9, 11, 14 and 19) resin formulations are shown in Figure 4b. Note that the non-linear stress-strain behavior, especially at higher strains, is suggestive of the hyper-elastic nature of the material. Normalized to mass, the 3DP-PDMS-S macromer had ~3.5 times more reactive (methacryloxypropyl) groups than 3DP-PDMS-E (Table S1, Supporting Information). Consequently, we hypothesize that an increase in E:S ratio lowers the degree of cross-linking in the polymer and increases the chain length between cross-links. Consistently with this hypothesis, the Young's modulus of 3DP-PDMS decreased with an increase in the E:S ratio, ranging between 937 kPa for E:S = 4 and 520 kPa for E:S=19 (Figure 4c). However, surprisingly, the photoinitiator concentration did not significantly alter the Young's modulus in any of the E:S ratios (Figure S4, Supporting Information) but it did affect the elongation-at-break values, specifically for E:S ratios of 14 and 19 (Figure 4d). We were able to optimize resins made with E:S ratios of 14 and 19 that yielded elastomers with elongation-at-break (143% and 159%, respectively) greater than Sylgard-184.

The thermal stability of the 3D-printed elastomeric structures is an important consideration for many applications. Since cell-based biomedical devices often require sterilization by autoclaving, we decided to investigate the effect of temperature (120 °C) on the mechanical properties of the 3DP-PDMS structures printed with the Sylgard-184-like E:S blends (as discussed in the previous paragraph). It has been shown before that due to greater degree of crosslinking at elevated temperatures, the Young's modulus of Sylgard-184 PDMS increases by ~86% and the elongation-at-break decreases by ~29% when heated to 125 °C[31]. After the printed 3DP-PDMS parts were heated to 120 °C for 12 hrs, the elongation-at-break decreased by 12.6% and 33.5% for the E:S = 14 and E:S = 19 blends, respectively; however the decreases were not statistically significant (Figure S5a, Supporting Information). Moreover, the Young's modulus also remained statistically unchanged at 120 °C (Figure S5b, Supporting Information), thereby demonstrating good thermal stability.

The solubility of 3DP-PDMS in organic solvents is a critical factor in determining the solvent(s) used in the post-processing of 3D-printed devices that contain voids (e.g. channels). The solvent has to be efficient in dissolving and removing uncured resin from channel/voids after printing. In addition, for cell-based applications, the solvent has to permeate the 3D-printed objects and extract the toxic photoinitiator, partially-cured macromers and other photopolymerization byproducts from the bulk of the devices.

However, if the solvent is too volatile, rapid deswelling can develop mechanical stresses and create cracks in the printed devices when the solvent is removed or exchanged. Therefore, we conducted a systematic study to characterize the swelling of 3DP-PDMS-S parts and dissolution of unbound photopolymerization byproducts in different organic solvents (Figure S6a, Supporting Information). Briefly, we measured the volumetric and mass change of photo-polymerized 3DP-PDMS-S cubes after being immersed in different solvents for 24 hrs. In a scatter plot, we plotted the swelling ratio ($\Delta V = (V_f - V_i)/V_i$) and the mass loss ($\Delta M = -(M_f - M_i)/M_i$) for each solvent (Figure S6b, Supporting Information). The 3DP-PDMS-S cubes swelled significantly more in hexane (72%), tetrahydrofuran (THF) (68%), and the volatile methylsiloxanes OS-20 and OS-10 (64%), than in acetone (13%) and isopropyl alcohol (IPA) (11%). However, the mass loss, which presumably comes from the dissolution of unbound polymerization byproducts, was very similar (~10–13%) for all the solvents except water. Therefore, for the purpose of dissolution of unbound byproducts (at least when dissolved over long periods of time), the higher swelling solvents did not provide a significant advantage over the low swelling solvents like acetone and IPA.

High gas permeability of PDMS is important in cell-based biomicrofluidic operations and therefore we sought to compare the oxygen permeability of our 3DP-PDMS resin to the conventional thermally cured Sylgard-184 PDMS (Figure S7, Supporting Information). We used an oxygen sensitive fluorophore, platinum(II) octaethylporphyrinketone (PtOEPK)[32], to compare the rate of oxygen diffusion into a sealed chamber through a 250 m membrane of commercial PDMS (BISCO HT-6240) and 3DP-PDMS-S (Figure S7a&b, Supporting Information). As the chamber is allowed to equilibrate to atmosphere from vacuum, the rate of fluorescence quenching is directly proportional to the flux of oxygen diffusing through the membrane (Figure S7c, Supporting Information). We found that the rate of fluorescent quenching after equilibration of HT-6240 and 3DP-PDMS-S membrane-covered chambers were $-32.82\ s^{-1}$ and $-29.86\ s^{-1}$ respectively, showing that they were similarly permeable to gases (Figure S7c, Supporting Information).

Cell-based applications warrant a stringent biocompatibility standard for SL-printed devices. The toxic photopolymerization byproducts as well as unreacted compounds that remain in the bulk of the SL-printed structures need to be extracted and removed from the devices before they are used for cell culture. Serial extraction with a number of organic solvents (e.g. xylenes, ethanol) has been previously reported to make Sylgard-184 PDMS-molded devices cytocompatible[33]. We performed a serial extraction of the SL-printed 3DP-PDMS-S petri dishes (Figure 5a, 5b) with the following solvents: xylene isomers (12 hrs), 1:1 xylene:IPA (8 hrs), IPA (16 hrs), followed by deionized water (8 hrs). The extracted petri dishes were then heated at 120 °C for 12 hrs (to remove any residual volatile components) and UV-treated for 2 hrs (to completely cure and sterilize). We cultured Chinese hamster ovary (CHO-K1) cells (a mammalian cell line used extensively in biotechnology) onto extracted and unextracted 3DP-PDMS-S dishes, as well as molded-PDMS (Sylgard-184, autoclaved) control dishes. Cells grown on solvent-extracted 3DP-PDMS-S dishes were morphologically indistinguishable from those cultured on Sylgard-184 dishes (Figure 5c), and showed excellent viability, statistically similar to Sylgard-184 dishes ($p > 0.1$, using Student's t-test) (Figure 5d). However, the unextracted 3DP-PDMS-S dishes showed a drastic, statistically-significant ($p < 0.01$, using Student's t-test), reduction (82%) in live cells (Figure 5e), which

proves that solvent extraction is an essential step for making SL-printed devices cytocompatible. The serial extraction protocol has not been optimized and shorter incubation times might be sufficient to completely remove the residual toxic components from the 3DP-PDMS-S dishes. Furthermore, the complexity, total volume and surface-to-volume ratio of the SL-printed devices might play a role in the time required for complete extraction. A viability assay performed every 24 hrs for 3 days showed statistically-insignificant difference ($p > 0.1$, using Student's t-test) in the total number of live cells between solvent-extracted 3DP-PDMS-S and Sylgard-184 dishes (Figure 5f). Therefore, the solvent-extracted 3DP-PDMS-S dishes can support long-term growth, proliferation and viability of mammalian cells.

We have developed and demonstrated the use of a SL-printable resin for manufacturing elastomeric parts having physical, optical and mechanical properties similar to the conventional thermally-cured elastomeric PDMS. For comparison purposes, we provide a table summarizing the properties of commercial and previously-reported elastomeric SL-resins (Table S3, Supporting Information). We envision that the progress made in SL-printed PDMS microdevices reported here, in combination with a new generation of higher-resolution SL printers, will soon pave the way towards digital manufacturing of cytocompatible microfluidic systems featuring elastomeric actuators and other advanced functionalities.

Experimental Section

Materials for resin formulation:

All the methacrylated silicone polymers and co-polymers – methacryloxypropyl terminated polydimethylsiloxane (CAS: 58130–03-3), 1000 cSt, [2–4% (methacryloxypropyl)methylsiloxane]-dimethylsiloxane copolymer (CAS: 104780–61-2) (1000–2000 cSt), [4–6% (methacryloxypropyl)methylsiloxane]-dimethylsiloxane copolymer (CAS: 104780–61-2) (8000–10000 cSt) and [7–9% (methacryloxypropyl)methylsiloxane]-dimethylsiloxane copolymer (CAS: 104780–61-2) (2000–3000 cSt) were purchased from Gelest Inc. (Morrisville, PA). Ethyl (2,4,6-trimethylbenzoyl) phenyl phosphinate (TPO-L) and 2-isopropyl thioxanthone (ITX) were generously offered as samples from Esstech Inc. (Essington, PA). Dow Corning OS-10 silicone fluid and Dow Corning OS-20 silicone fluid, and Dynaloy Dynasolve M-10 cleaner fluid were purchased from Ellsworth Adhesives (Germantown, WI). Isopropyl alcohol (IPA), 3-(trimethoxysilyl)propyl methacrylate (TMSPMA), ethyl alcohol, acetone, n-hexane, methyl ethyl ketone (MEK), methyl isobutyl ketone (MIBK), toluene, xylenes and tetrahydrofuran (THF) were purchased from Sigma-Aldrich (St Louis, MO).

UV LED DLP stereolithography:

We used an Ilios HD 3D printer for all the stereolithography prints shown in this paper. The printer was fitted with HT stepper motors, which were controlled by an Arduino board and had a nominal Z-resolution of 12.5 μm. To minimize the use of resin for every printing run, we custom designed an 8.5 cm × 8.5 cm vat fitted with a 0.25-in. thick quartz plate at the bottom. A 0.002-in. Teflon film tape (CS Hyde Inc.) was attached to the quartz plate of the

vat to prevent the polymerized PDMS from sticking to the vat. The build plate was also redesigned to have an area of 8 cm × 6 cm, which can fit inside the new vat as well as hold a 5 cm × 7.5 cm glass slide, which is typically used as the surface for building our prints. Both the vat and the build plate were CNC-machined (Proto Labs Inc., Maple Plains, MN) with aluminum 6061 and black-anodized (ASKO Processing Inc., Seattle, WA) to make it resistant to corrosion. For the projector, we used the Wintech Pro4500, a 385 nm UV LED projector based on the DLP4500 chipset from Texas Instruments. The printing area of the DLP was 65.6 mm × 41 mm and consisted of 1280 × 800 pixels, which resulted in a single pixel having projected dimensions of 51.25 μm × 51.25 μm.

CAD designs of the prints were made with Autodesk Inventor® and exported as a STL file. We used Creative Workshop® software to import the STL design file and digitally slice it into a sequence of image (JPG) files that typically contain only black or white pixels. However, any of these images can be digitally edited to change the grayscale level in order to spatially modulate the exposure levels for any given layer.

Before starting the print, the PDMS resin (~30–40 mL) was poured into the vat. Glass slides (5 cm × 7.5 cm) were used as substrates for building the prints. The slides were sequentially cleaned with acetone, isopropyl alcohol and water, and dried in a 70 °C oven. To facilitate the adhesion of the polymerized 3DP-PDMS prints to the glass substrates, we coated the glass slides with 3-(trimethoxysilyl)propyl methacrylate (TMSPMA) (Sigma-Aldrich). We placed the cleaned glass slides on a 85 °C hot plate with a paper soaked with ~0.5 mL of 3-(trimethoxysilyl)propyl methacrylate (TMSPMA) for 8 hrs. The 3DP-PDMS resin was applied to one side of a glass slide, which was then attached to the build plate with a brief UV exposure using a broadband UV lamp (B-100 A, UVP).

A custom MATLAB script controlled the entire 3D-printing process from the movement of the Z-motors to control of the DLP system. The software can specify and precisely control the layer thickness, the LED intensity, the exposure time for each layer, the separation distance and Z-motor speed.

After the printing was completed, the glass slide with the printed object was detached from the build plate (using a razor blade). The uncured 3DP-PDMS resin was rinsed off by immersing in an isopropyl alcohol bath. For microfluidic devices or for prints with internal voids under overhanging structures (bridges, hollow solids), we first used compressed air to blow-off excess resin, and then sequentially flowed in Dynasolve M10 and isopropyl alcohol using a syringe to rinse off the uncured resin. A vacuum source was used to aspirate out the solvents from the internal voids. The rinsing and aspiration process was continued till the internal channels or voids were cleared of uncured resin.

Mechanical testing:

Mechanical testing was carried out using an Instron 5584H Load Frame equipped with a 50 N load cell. We fabricated dog-bone-shaped specimens (mid-section dimensions: 1 cm × 3 mm × 3 mm) using different resin formulations (Figure 2a), subjected them to tensile stress along their longitudinal axis and tested at a displacement rate of 10 mm/min. The elongation of the specimen was recorded using a video axial extensometer (Movie S2, Supporting

Information). The Young's modulus was determined from the slope of the initial linear segment of the stress-strain curve (axial strain below 40%).

Solvent compatibility measurements:

A required post-processing step of SL-printing involves the removal of residual resin from around the prints using a solvent. Since it is difficult to control the time required to completely remove the uncured residual resin with a solvent, for these measurements we molded the cubes instead, since molding does not require solvent exposure after fabrication. First, a template with 5 mm cubes was SL-printed onto a glass slide using PEG-DA-258 as the resin. An agarose mold was then prepared by pouring a 2% agarose solution on to the PEG-DA-258 template. The thickness of the agarose mold was constrained by putting a slab of PDMS on top. After cooling the solidified agarose gel was taken out of the PEG-DA-258 mold and stored in water. The agarose mold was then placed on a glass slide with a Teflon tape adhered to its surface. The 3DP-PDMS-S resin (0.6% TPO-L) was carefully dispensed with a dropper into the cube-shaped holes in the agarose mold, and a sheet of Mylar was placed on top. The Mylar sheet ensured that the top surface of the 3DP-PDMS cubes were flat and of the same height as the agarose mold. The entire assembly was then placed in a UV-transilluminator box for 5 min, which was sufficient to cure through the entire height of the resin. The Mylar sheet was then peeled off, and the agarose gel was slowly lifted off the Teflon-surface on the glass slide, leaving behind the 3DP-PDMS cubes. The 3DP-PDMS cubes were inspected and those with defects like bubbles in the bulk volume or non-uniform edges were discarded.

The cubes were weighed using a lab balance to give us the initial mass (M_i). The cubes were then placed in 5 mL of the solvent in a glass vial and immediately imaged using a stereomicroscope. The length of the cube edges measured using ImageJ gave us the initial volume (V_i). The cubes were kept submerged in the solvents for 24 hrs. Then they were imaged again and the length of the edges measured to give us the final (swollen) volume (V_f). The swelling ratio was determined by the ratio of the final (swollen) to the initial volume. The solvents in the vial were sequentially diluted with isopropyl alcohol (IPA), till the original solvent was reduced to 6.25%. Heating at 120 °C for 24 hrs then evaporated off the remaining solvent. After all the solvent was evaporated, the cubes were weighed again to give the final mass (M_f). The mass loss was determined by the decrease in mass expressed as a percentage of the initial mass.

Gas permeability measurements:

To test the gas permeability of the printed PDMS sheet, an O_2 permeability test device was fabricated. The O_2 permeability test device consisted of two parts - a platinum-based O_2 sensor, and a 3D-printed vacuum chamber. The platinum-based O_2 sensor was fabricated by dissolving 1 mg/mL platinum(II) octaethylporphine ketone (PtOEPK, Santa Cruz Biotechnology, Inc) in 20% (w/v) polystyrene in toluene[32]. The PtOEPK solution was sealed in the glass bottle to prevent evaporation and dissolved using a magnetic stirrer for 24 hrs. Completely dissolved oxygen-sensing dye was coated on a Mylar film. Evaporation of the toluene resulted in a polystyrene thin film with embedded PtOEPK. The fabricated PtOEPK oxygen sensor was diced into 1 cm square pieces. The 3D-printed vacuum chamber

(3 cm (w) × 3 cm (l) × 1 cm (h)) was designed with Autodesk Inventor® and fabricated using an Ember® DLP 3D Printer (Autodesk, INC) in poly(ethylene glycol) diacrylate (MW=258) (PEG-DA-258) (Sigma Aldrich) mixed with 0.6% w/w Irgarcure 819 (IRG) (BASF Corporation) as a photoinitiator and 0.6% w/w 2-isopropylthioxanthone (ITX) (Esstech Inc.) as a photosensitizer. The PtOEPK polystyrene film was placed at the bottom of the vacuum chamber, which was then sealed by bonding a 250 μm PDMS membrane on top. Vacuum was applied to the sealed chamber and a PET film was placed on top to prevent air flow through the PDMS membrane. The vacuum line was closed after 30 sec and the PET film was removed to observe the gas permeability of the PDMS membrane. The fluorescent intensity of the PtOEPK sensor was quenched by O_2 diffusing into the chamber through the PDMS membrane, and the rate of fluorescence decay indicated the permeability of the PDMS membrane. An inverted epifluorescence microscope (Nikon Eclipse Ti) was used for image acquisition and analysis. Images were taken with Plan Fluor 10x objective.

Cell culture and viability assay:

Chinese hamster ovary cells (CHO-K1) were cultured in DMEM media (Invitrogen) supplemented with 10% fetal bovine serum (Hyclone), 1% penicillin-streptomycin (Invitrogen) and 2 mM L-glutamine (Sigma-Aldrich). The cells were grown in an incubator with 5% CO_2 at 37 °C. After 24–72 hrs of growth, the cells were removed from the petri dishes using 0.05% Trypsin-EDTA, and the viability of the culture was assessed using the Trypan Blue exclusion assay. Live cell staining of an adherent CHO-K1 culture was performed by replacing the growth media with serum-free DMEM supplemented with 4 μM Calcein Green AM, 4 μM Ethidium homodimer, and 1 μM Hoechst 33342 (all from Invitrogen). After incubation at 37 °C for 30 mins, the staining solution was aspirated out and replaced with Fluorobrite (Invitrogen) media to ensure minimal background fluorescence when imaging.

Microfluidic operation:

For the microfluidic experiments, we used a Chemyx Fusion 720 syringe pump. Syringes (5 mL, BD Biosciences) were loaded with the different dyes and connected to the inlets of the SL-printed microfluidic device. The inlet holes were designed to fit the outer diameter of silicone tubings (Cole-Parmer), which ensured a tight leak-proof connection.

Microscopy:

We used a Nikon SMZ1500 stereomicroscope fitted with a Canon Rebel DSLR camera for the imaging of 3D-printed devices and structures. We used an inverted Nikon TE3000 epifluorescence microscope for all the phase contrast and fluorescence imaging of cells. We used ImageJ for analyzing images and making measurements.

Statistical Analysis:

We used MATLAB Statistical Toolbox to perform our statistical tests. We performed unpaired two-tailed independent samples Student’s t-test on the cell viability (Figure 5) and thermal effect data (Figure S5, Supporting Information). We compared the Young’s modulus and elongation-at-break between the multiple E:S 3DP-PDMS resin blend groups (Figure 4)

using one-way ANOVA. Post-hoc analysis to determine statistical significance between pairs of groups was performed by the Tukey-Kramer test.

Derivation of Cure-Depth versus Exposure Time Relation from Beer-Lambert Law

According to the Beer-Lambert law, the absorbance of the resin linearly depends on the molar absorptivity (ε) and concentration (c) of the absorbing species present in the resin.

$$I\left(z\right) = I_0 e^{-2.303\left(\varepsilon_i c_i + \varepsilon_a c_a\right)z} \quad (1)$$

where $I(z)$ is the intensity at a depth z, I_0 is the intensity at z=0, ε_i and c_i are the molar absorptivity and concentration of the photoinitiator, respectively, and ε_a and c_a are the molar absorptivity and concentration of the UV-absorber (or photosensitizer), respectively.

Let us assume that the resin requires a threshold dose of energy (E_c) for curing, and the minimum time required for the resin to start curing at the surface closest to the light source (which receives the maximum intensity I_0) is T_0. Therefore,

$$I_0 = \frac{E_c}{T_0} \quad (2)$$

Let us also assume that z_c is the total depth of the resin that is polymerized (cure-depth) when the exposure time is t_c. Therefore, the energy at a depth z_c must be the threshold energy E_c, or

$$I\left(z\right) = \frac{E_c}{t_c} \quad (3)$$

Using equations (2) and (3) in equation (1), we can show that the cure-depth, z_c, is linearly related to the logarithm of the exposure time, t_c, according to the following equation,

$$z_c = h_p \ln\left(\frac{t_c}{T_0}\right) \quad (4)$$

where h_p is the characteristic penetration depth defined by

$$h_p = 1/2.303\left(\varepsilon_i c_i + \varepsilon_a c_a\right) \quad (5)$$

The slope of a log-linear plot of z_c and t_c will therefore give the characteristic penetration depth of the resin.

Supplementary Material

Refer to Web version on PubMed Central for supplementary material.

Acknowledgements

The authors would like to acknowledge the National Institutes of Health (grant number R01NS064387) and the National Cancer Institute (grant number R01CA181445) for partially supporting this work. C.P. was a recipient of a “Consejo Nacional de Ciencia y Tecnologia” (CONACYT) Mexican fellowship. Y.T.K was partially supported by the BioNano Health-Guard Research Center, which is funded by the Ministry of Science, ICT (MSIT) of Korea as Global Frontier Project (Grant No. H-GUARD_2014M3A6B2060302). The authors would also like to thank Bill Kuykendall for help with material testing.

References

[1]. Xia Y, Whitesides GM, Annu. Rev. Mater. Sci. 1998, 28, 153.

[2]. Bhattacharjee N, Urrios A, Kang S, Folch A, Lab Chip 2016, 16, 1720. [PubMed: 27101171]

[3]. Kong YL, Tamargo IA, Kim H, Johnson BN, Gupta MK, Koh TW, Chin HA, Steingart DA, Rand BP, McAlpine MC, Nano Lett 2014, 14, 7017. [PubMed: 25360485]

[4]. Muth JT, Vogt DM, Truby RL, Mengüç Y, Kolesky DB, Wood RJ, Lewis JA, Adv. Mater. 2014, 26, 6307. [PubMed: 24934143]

[5]. Kolesky DB, Homan KA, Skylar-Scott MA, Lewis JA, Proc. Natl. Acad. Sci. 2016, 113, 3179. [PubMed: 26951646]

[6]. Roh S, Parekh DP, Bharti B, Stoyanov SD, Velev OD, Adv. Mater. 2017, 29.

[7]. Corbel S, Dufaud O, Roques-Carmes T, in Stereolithography Mater. Process. Appl. (Ed.: Bartolo PJ), Springer, 2011, pp. 141–160.

[8]. Choi KM, Rogers JA, J. Am. Chem. Soc. 2003, 125, 4060. [PubMed: 12670222]

[9]. Bhagat AAS, Jothimuthu P, Papautsky I, Lab Chip 2007, 7, 1192. [PubMed: 17713619]

[10]. Desai SP, Taff BM, Voldman J, Langmuir 2008, 24, 575. [PubMed: 18081333]

[11]. Cong H, Pan T, Adv. Funct. Mater. 2008, 18, 1912.

[12]. Coenjarts CA, Ober CK, Chem. Mater. 2004, 16, 5556.

[13]. Rekštytė S, Malinauskas M, Juodkazis S, Opt. Express 2013, 21, 17028. [PubMed: 23938551]

[14]. Thrasher CJ, Schwartz JJ, Boydston AJ, ACS Appl. Mater. Interfaces 2017, 9, 39708. [PubMed: 29039648]

[15]. Patel DK, Sakhaei AH, Layani M, Zhang B, Ge Q, Magdassi S, Adv. Mater. 2017, 29.

[16]. Fink JK, Reactive Polymers: Fundamentals and Applications, Elsevier, 2013.

[17]. Moad G, Solomon DH, The Chemistry of Radical Polymerization, Elsevier, 2005.

[18]. Green WA, Industrial Photoinitiators - A Technical Guide, CRC Press, 2010.

[19]. Fouassier JP, Allonas X, Lalevée J, Dietlin C, in Photochem. Photophysics Polym. Mater. (Ed.: Allen NS), Wiley, Hoboken, 2010, pp. 351–419.

[20]. Urrios A, Parra-Cabrera C, Bhattacharjee N, Gonzalez-Suarez AM, Rigat-Brugarolas LG, Nallapatti U, Samitier J, Deforest CA, Posas F, Garcia-Cordero JL, Folch A, Lab Chip 2016, 16.

[21]. Hinton TJ, Hudson A, Pusch K, Lee A, Feinberg AW, ACS Biomater. Sci. Eng. 2016, 2, 1781. [PubMed: 27747289]

[22]. Sun C, Fang N, Wu DM, Zhang X, Sensors Actuators A Phys. 2005, 121, 113.

[23]. Fang N, Sun C, Zhang X, Appl. Phys. A Mater. Sci. Process. 2004, 79, 1839.

[24]. Gong H, Beauchamp M, Perry S, Woolley AT, Nordin GP, RSC Adv. 2015, 5, 106621. [PubMed: 26744624]

[25]. Kitson PJ, Rosnes MH, Sans V, Dragone V, Cronin L, Lab Chip 2012, 12, 3267. [PubMed: 22875258]

[26]. Gong H, Bickham BP, Woolley AT, Nordin GP, Lab Chip 2017, 17, 2899. [PubMed: 28726927]

[27]. Tan JL, Tien J, Pirone DM, Gray DS, Bhadriraju K, Chen CS, Proc. Natl. Acad. Sci. 2003, 100, 1484. [PubMed: 12552122]

[28]. Thorsen T, Maerkl SJ, Quake SR, Science (80-.). 2002, 298, 5593.

[29]. Cooksey GA, Sip CG, Folch A, Lab Chip 2009, 9, 417. [PubMed: 19156291]

[30]. Lai H, Folch A, Lab Chip 2011, 11, 336. [PubMed: 20957288]

[31]. Johnston ID, McCluskey DK, Tan CKL, Tracey MC,J. Micromechanics Microengineering 2014, 24, 35017.

[32]. Sinkala E, Eddington DT, Lab Chip 2010, 10, 3291. [PubMed: 20938500]

[33]. Lee JN, Park C, Whitesides GM, Anal. Chem. 2003, 75, 6544. [PubMed: 14640726]

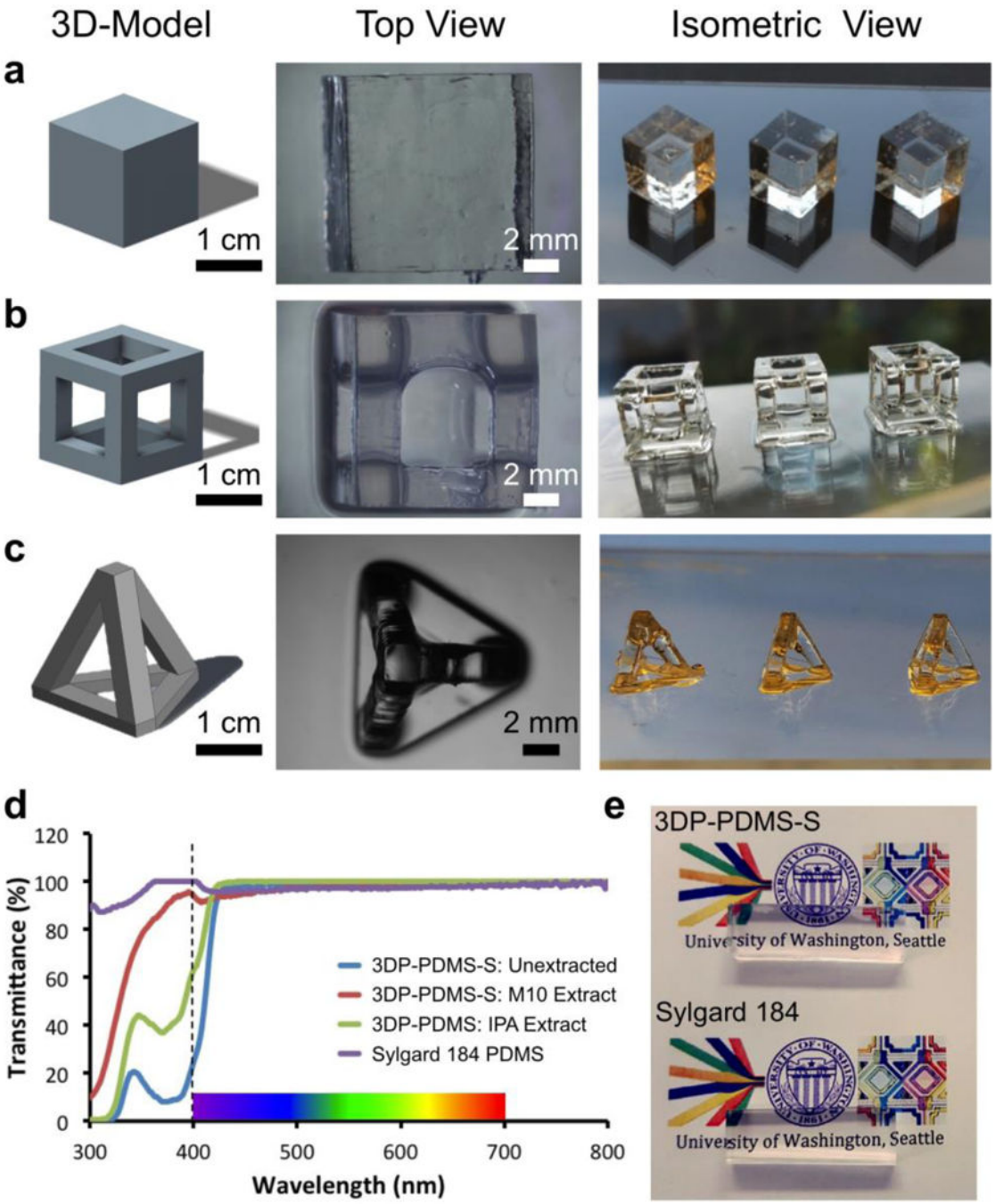

Figure 1. Transparent SL prints with 3DP-PDMS-S resin

(using 0.6% TPO-L). CAD model, top view and isometric view of (a) solid cubes, (b) hollow cubes and (c) hollow tetrahedrons. (d) Transmittance of samples of molded Sylgard-184 PDMS, freshly printed 3DP-PDMS-S, isopropyl alcohol (IPA) extracted 3DP-PDMS-S print, and Dynasolve M10 extracted 3DP-PDMS-S print. (e) Comparison of the transparency of 4 mm-thick rectangular blocks of PDMS placed over printed text (Calibri 10-pt) and color images – one 3D-printed with 3DP-PDMS-S resin (top) and the other molded with Sylgard-184 (bottom).

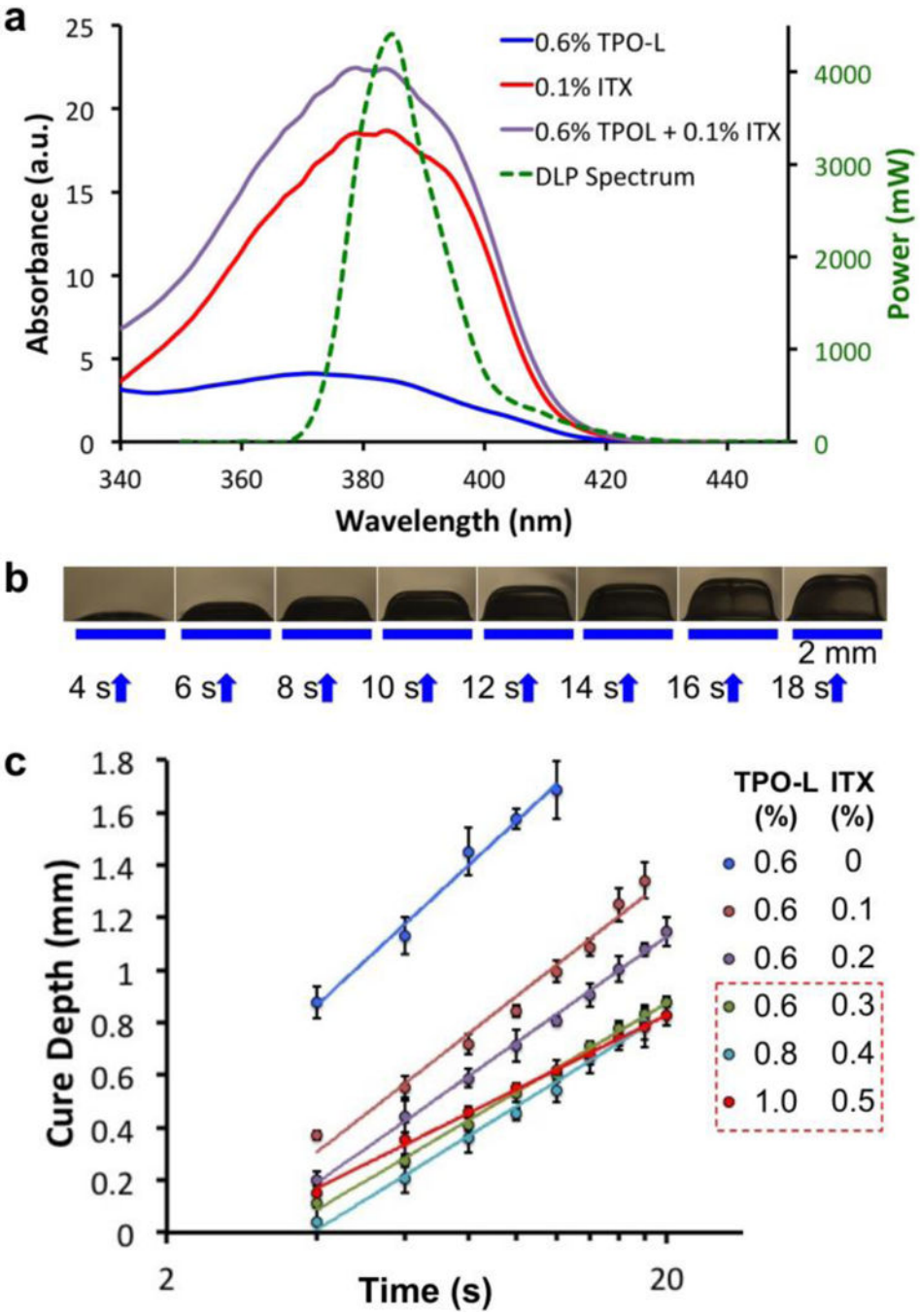

Figure 2. Resin absorbance and Z-Resolution of SL-printing.

(a) Absorbance measurements of the photoinitiator TPO-L (0.6%) alone, the photosensitizer ITX (0.1%) alone and the 0.6% TPO-L + 0.1% ITX mixture, compared with the power spectrum (green) of the UV-LED source used in the DLP SL-printer. (b) Cure depth determination: 2 mm wide lines of 3DP-PDMS (with 0.6% TPO-L and 0.3% ITX) formed after being exposed with 385 nm UV for different periods of time. (c) Log-linear plot of the cure-depth versus exposure time for different concentrations of TPO-L and ITX ($n \geq 3$). The solid lines denote the logarithmic fits of the data points ($R^2 \geq 98.5\%$ for all the fits). The

slopes of the lines determine the characteristic penetration depth of the resins. Error bars represent SEM. Of the three resins that have the smallest slopes (boxed), we chose the mixture with 0.6% TPO-L and 0.3% ITX because it produced the most transparent prints (see text).

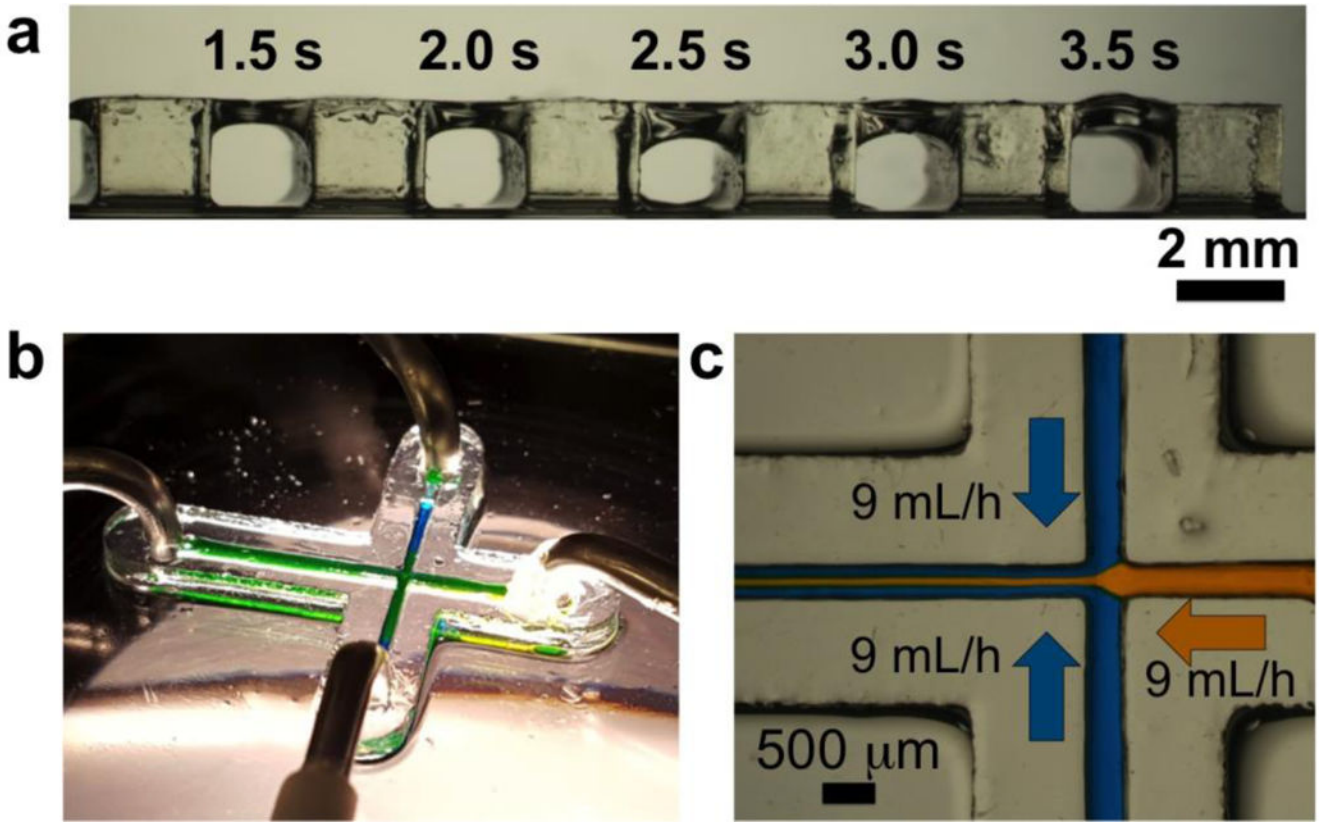

Figure 3. Microfluidic devices with 3DP-PDMS SL-printing.

(a) Bridge structures printed with 3DP-PDMS: Characterization of exposure times required for creating roof structures on top of voids. The walls (2 mm wide, 2 mm high) are 3D-printed and the intervening areas are exposed with UV for different times. The uncured resin from the voids was later cleared with isopropyl alcohol. (b) A microfluidic device with 500 μm wide channels SL-printed with 3DP-PDMS. (c) A central stream of yellow dye (9 mL/hr) flanked by two streams of blue dye (9 mL/hr each) produce a heterogeneous laminar flow (9 mL/hr) in the 3DP-PDMS microfluidic device.

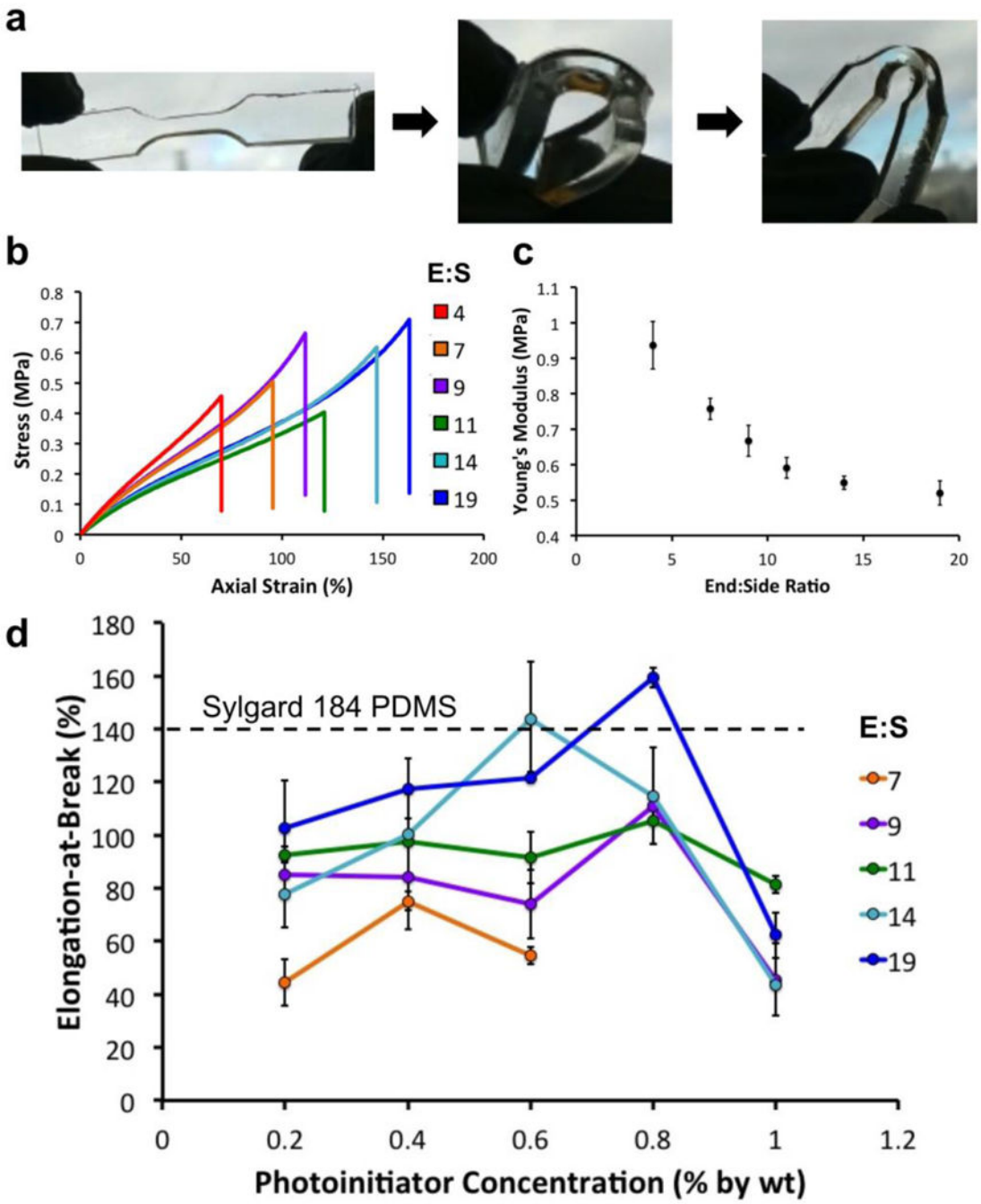

Figure 4. Mechanical Characterization of 3DP-PDMS.

(a) 3D printed flexible dog-bone structure made with 3DP-PDMS. (b) Representative stress-strain curves of dog-bone specimens printed with 3DP-PDMS prepared with different ratios of end group and side-chain macromers. (c) Young's modulus of 3DP-PDMS prepared with different ratios of end group and side-chain macromers. Error bars are SEM. (d) Elongation at break values of 3DP-PDMS prepared with different ratios of end group and side-chain macromers and different photoinitiator concentrations. Error bars are standard deviations. The elongation-at-break of Sylgard-184 PDMS is shown as a dotted line.

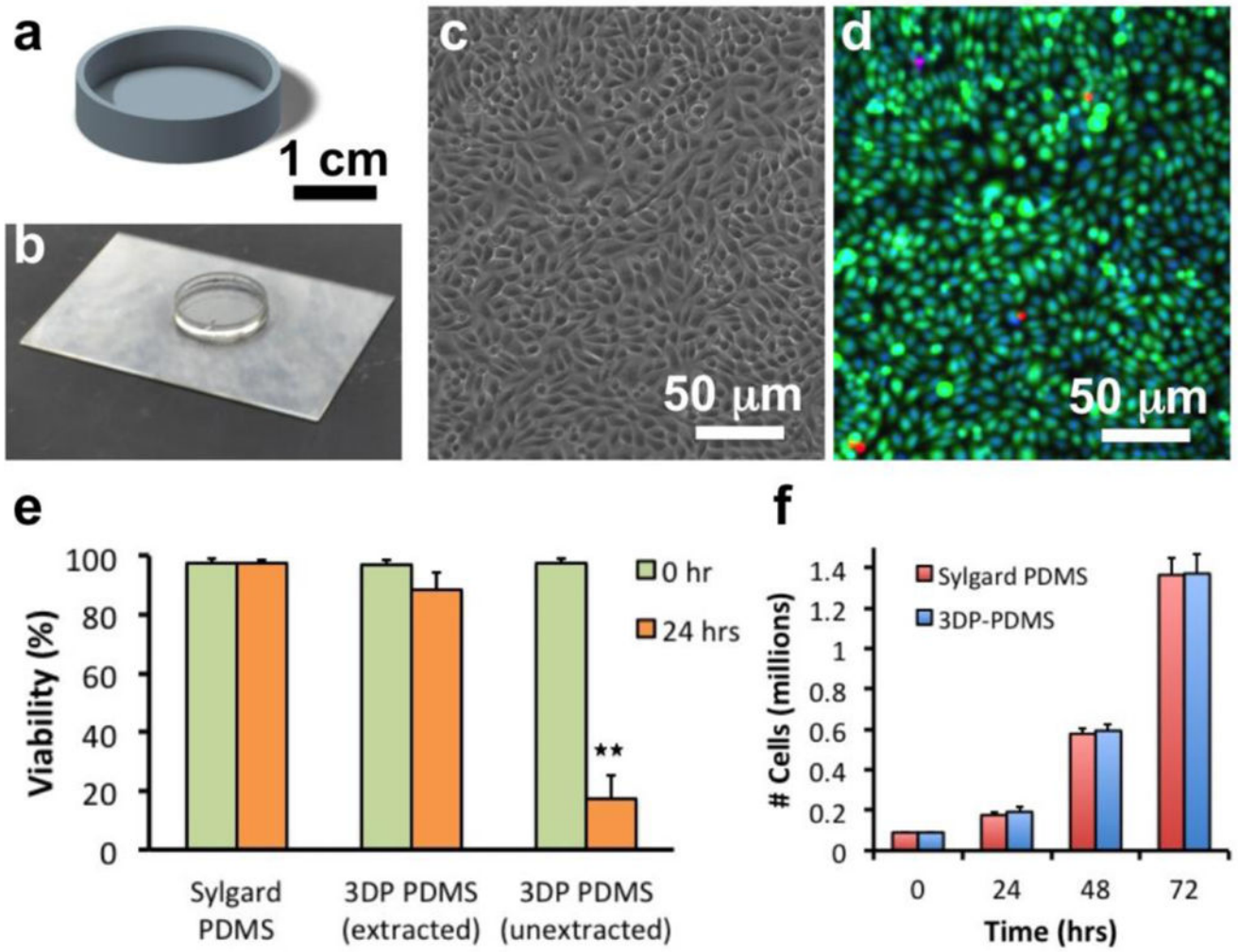

Figure 5. Biocompatibility of SL-printed 3DP-PDMS-S.

(a) CAD design of a 30 mm diameter petri dish. (b) SL-printed PDMS petri dish. (c) Phase-contrast micrograph of CHO-K1 cells cultured on a solvent-extracted 3DP-PDMS petri dish after 24 hrs. (d) Merged fluorescence micrograph of CHO-K1 cells stained with Calcein Green AM (5 μM) (green), Ethidium homodimer 1 (4 μM) (red) and Hoechst 33342 (1 μM) (blue). (e) Comparison of viability of CHO-K1 cells after 24 hrs of culture on a Sylgard-184 thermally cured PDMS disc, a solvent-extracted SL-printed 3DP-PDMS-S petri dish and an unextracted SL-printed 3DP-PDMS-S petri dish. Error bars denote SEM ($n \geq 3$). Double asterisk (**) denotes $p < 0.01$ when using unpaired two-tailed Student's t-test to determine statistical significance. (f) Bar graph of the number of live cells on Sylgard-184 PDMS disc and solvent- extracted SL-printed 3DP-PDMS-S petri dish after every 24 hours for 3 days. Error bars denote SEM ($n \geq 3$). There was no statistical difference in the mean number of total live cells at the end of each day (unpaired two-tailed Student's t-test).